2023 62nd IEEE Conference on Decision and Control (CDC)
December 13-15, 2023. Marina Bay Sands, Singapore

Lyapunov based Time Varying Subregional Control of System with Distributed Parameters

André Heining and Oliver Sawodny

***Abstract*— An increased size of optical reflective elements, e.g., in the trend of large telescopes, requires thin structures to maintain a little mass for regaining performance in a change of orientation for example. However, exciting such a compliant structure leads to vibrations. Often, the whole surface is actively damped, although only a subregion might be exposed. Thus, a state feedback for the control of a subregion is derived by utilizing a Lyapunov function, deduced from mechanical energy. The method is then extended towards a time varying subregion. A simulation of a vibrating thin circular plate shows that the proposed method outperforms a linear quadratic regulator and that the time varying feedback law renders the closed loop stable.**

I. INTRODUCTION

The strive for an increased resolution in optical applications demands for larger reflective surfaces to capture more light [3], [6], [10]. Due to dynamic and monetary aspects, structures of increasing size shall be lightweight. This, however, leads to structures with thin elements, inheriting low natural frequencies and flexural rigidity. Thus, a change in the pose of the optical element excites the system what results in a vibrating response and, hence, aberrations.

Often, the whole surface is actively damped to ensure a little surface deviation and, hence, little aberrations. However, due to manufacturing, e.g., discharge areas in polishing, and assembly aspects, e.g., actuator mounts, only a subregion of the surface is exposed and needs to be controlled. This region might also change with pose in conjunction with the beam shape, see Figure 1. Hence, a time varying subregional control of the elastic flexure is of interest.

A. Related Work

Controlling systems with distributed parameters over the whole and a partial domain has been of interest for many decades. The contributions of [4] and [5] deal with effect of the actuator location and input characteristic on the controlability of distributed systems over the whole domain and a subregion. Conditions on strategic locations and the amount of actuators and sensors are derived and illustrated by various examples.

In order to derive an analytic control law that covers all infinitely many plate modes, a boundary control together with a Lyapunov functional to show stability is often utilized. The work of [11] and its extension [12] deals with boundary control of a vibrating plate. First a thorough stability analysis by using a Lyapunov functional is performed in [11] and a nonlinear robust boundary control law is evaluated in a simulation study. In [12], an extended state observer on the active boundary and a Lyapunov redesign for a stable and adaptive control gain are considered to achieve a robust active disturbance rejection for a rectangular shaped plate with two neighboring edges being clamped. The Lyapunov functional covers the mechanical energy of the plate and actuator mass. Numerical examples show an improved behavior of the adaptive control law, since an upper bound of the disturbance estimation is not required.

Another example is presented in [7]. The author considers a variable structural control for a thin flexible plate with viscoelastic boundary conditions based on a semi group approach. The derived sliding mode control, which acts on the boundary of the plate, leads to an exponentially stable closed loop.

A different boundary control approach for a system with distributed parameters is given by the authors of [8] and [9]. In [8] a boundary controller and observer for a slender Timoshenko beam are designed by exploiting backstepping methods. The stability of the derived controller and observer is then shown by consulting Lyapunov function candidates in [9]. Moreover, conducted simulations underline the efficiency of the developed method.

By considering a distributed control input as well, an optimal control for a subregion of a vibrating plate described by a bilinear system is derived in [1] and its extension [2]. Based on a cost function, covering the input signal and the deviation between the desired and actual shape of the region, an algorithm for the optimal control input is deduced. Findings show a decrease in the control cost and error with decreasing size of the subregion.

However, computing the optimal control signal requires an iterative optimization in every time step, jeopardizing the real time applicability for systems requiring a high sampling frequency. Thus, we aim for deriving a closed form control law for actively damping a time varying subregion of a vibrating plate.

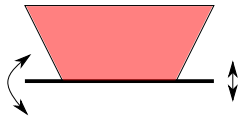

Fig. 1. Partially exposed surface of a plate that can change its pose in vertical and angular orientation. The light is colored in red.

A Heining and O. Sawodny are with Institute for System Dynamics, University of Stuttgart, Waldburgstr. 19, 70653 Stuttgart, Germany {heining, sawodny}@isys.uni-stuttgart.de

B. Contribution and Structure

By considering a general description of a thin plate, whose solution is expressed by modal analysis and synthesis and approximated by a truncation, a stabilizing feedback is derived by using a Lyapunov functional. The functional is deduced from the mechanical plate energy over the subregion of interest by using an approximate description of the surface deviation and an evaluation of the energy integral over finitely many grid points. Additionally, the method is extended to a time varying subregion and applied to a vibrating thin circular plate in a simulation study.

Therefore, the remaining paper is structured as follows: In Section II a general description of a thin circular plate and its modal solution is introduced. Building on Section II, conditions for regional controllability and a state feedback law for a fixed and time varying subregion based on a Lyapunov functional are presented in Section III. The derived results are than applied to a thin circular plate in Section IV and compared to a linear quadratic regulator, as the state of the art. Lastly a conclusion is drawn and an outlook for future research is given in Section V.

II. System description

The dynamic behavior of a thin plate's surface deviation $w(t,x,y)$ is governed by the partial differential equation (PDE) [13]

$$D\Delta\Delta w + Q_\mathrm{d} + \rho h \frac{\partial^2 w}{\partial t^2} = Q_a, \;\; t>0, \;\; (x,y)\in\Omega, \tag{1a}$$

$$\mathscr{M} w = M(x,y,t), \;\; t>0, \;\; (x,y)\in\partial\Omega, \tag{1b}$$

$$\mathscr{V} w = V(x,y,t), \;\; t>0, \;\; (x,y)\in\partial\Omega, \tag{1c}$$

$$w = \frac{\partial w}{\partial t} = 0 \;\text{ for }\; t=0, \;\; (x,y)\in\Omega, \tag{1d}$$

with the density ρ, plate thickness h and the rigidity D

$$D = \frac{Eh^3}{12(1-\nu^2)}, \tag{2}$$

with modulus of elasticity E, Poisson's ratio ν and plate thickness h. Moreover, the set of equations (1) include the Laplace operator Δ, actuator forces Q_a, a damping term Q_d, the operators $\mathscr{M}$ and $\mathscr{V}$ for the boundary moment $M(x,y,t)$ and the transversal force $V(x,y,t)$ as well as the plate surface Ω and its boundary $\partial\Omega$, see Figure 2. The actuator forces Q_a comprise the applied force $u_i(t)$ as well as the input characteristic $g_i(x,y)$ such that

$$Q_a(t,x,y) = \sum_{i=1}^{N_\mathrm{a}} g_i(x,y)u_i(t), \tag{3}$$

for $N_\mathrm{a}\in\mathbb{N}_+$ actuators. Note, that the arguments of $w(t,x,y)$ have been neglected in (1) due to readability.

A. Modal Analysis and Synthesis

A solution to (1) can be obtained by applying a modal analysis defined by

$$q_n(t) = \iint_\Omega w(t,\cdot)\psi_n(\cdot)\mathrm{d}\Omega \tag{4}$$

with modal amplitude $q_n(t)$ and the corresponding self-adjoint eigenmode $\psi_n(x,y)$. Furthermore, the eigenmodes are normalized such that

$$\iint_\Omega \psi_n(\cdot)\psi_m(\cdot)\mathrm{d}\Omega = \delta_{mn}, \tag{5}$$

with $\delta_{mn}=1$ for $m=n$ and zero elsewhere. The surface deviation of the plate is then obtained by superposing all eigenmodes scaled by their amplitude

$$w(t,\cdot) = \sum_{i=1}^{\infty} \psi_i(\cdot)q_i(t). \tag{6}$$

However, only a finite amount of $N\in\mathbb{N}_+$ modes can be evaluated, what leads to

$$w(t,\cdot) \approx \sum_{i=1}^{N} \psi_i(\cdot)q_i(t), \tag{7}$$

as an approximation of the real deviation.

Besides the spatial eigenmodes $\psi_n(\cdot)$, the modal analysis returns a set of ordinary differential equations (ODEs) for the time evolution of the modal amplitudes:

$$\ddot{q}_n(t) + 2d_n\omega_n\dot{q}(t)_n + \omega_n^2 q(t) = \tilde{u}, \;\; \forall \;\; t>0, \tag{8a}$$

$$q_n(t) = \dot{q}_n(t) = \ddot{q}_n(t) = 0, \;\; t=0, \tag{8b}$$

with the modal damping coefficient d_n, the natural frequency ω_n and modal actuator forces given by

$$\tilde{u}_n(t) = \iint_\Omega Q_\mathrm{a}(t,\cdot)\psi_n(\cdot)\mathrm{d}\Omega. \tag{9}$$

Gathering the modal amplitudes in a state vector

$$\boldsymbol{x}_\mathrm{e}(t) = (q_1, \;\; \dot{q}_1, \;\; ..., q_N, \;\; \dot{q}_N)^\mathsf{T} \tag{10}$$

results in the state space description

$$\dot{\boldsymbol{x}}_\mathrm{e}(t) = \boldsymbol{A}_\mathrm{e}\boldsymbol{x}_\mathrm{e}(t) + \boldsymbol{B}_\mathrm{e}\boldsymbol{u}(t), \tag{11}$$

with dynamic matrix $\boldsymbol{A}_\mathrm{e}$ and input matrix $\boldsymbol{B}_\mathrm{e}$.

III. Subregional Control

Next, the proposed modal synthesis and state space description is used to derive a feedback law for controlling only a subregion $\omega\subseteq\Omega$ of the plate surface. Since an empty region would result in an undefined control goal and would not have any benefits on an aberration improvement, a surface integral greater zero is assumed, which is captured

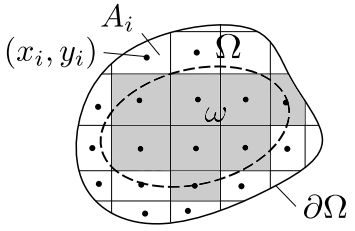

Fig. 2. Plate with surface domain Ω, boundary $\partial\Omega$ and subregion ω (dashed). The plate surface is subdivided into N_g segments with the center (x_i,y_i) of each segment i and corresponding area A_i. Grey segments are used to evaluate the mechanical plate energy over ω.

in the following assumption.

Assumption 3.1: The subregion that is subject to be controlled is star shaped and not empty, i.e.,

$$\iint_{\omega} \mathrm{d}\omega > 0. \tag{12}$$

Besides a non-empty subregion, actuators with their specific input characteristic need to be placed such that controllability of the region ω is ensured. Hence, necessary definitions and requirements are introduced in the following subsection.

A. Regional Controllability

In order to achieve a desired surface profile of a subregion of the considered plate (1), controllability of this area is necessary. Since a representation of the plate's surface deflection by a truncated modal synthesis (7) is an approximation of the deflection (6), the property of *weakly regionally controllability* is required which is defined as

Definition 3.2 ((2) [5]): The system (1) is said to be *weakly regionally controllable* to $\boldsymbol{z}_\mathrm{d} \in L^2(\omega)$ if, given $\varepsilon > 0$, there exists a control $\boldsymbol{u} \in L^2(0,T;\mathbb{R}^m)$ such that

$$\|\boldsymbol{z}(T,\boldsymbol{u})|_\omega - \boldsymbol{z}_\mathrm{d}\|_{L^2(\omega)} \leq \varepsilon, \tag{13}$$

where $\boldsymbol{z}(\cdot,u)$ includes the solution w of (1) and desired derivatives and $\boldsymbol{z}|_\omega$ is the restriction of $\boldsymbol{z}$ to ω.

Given Definition 3.2, an actuator configuration needs to be identified that achieves this property. Such a configuration is called ω-strategic and is defined as

Definition 3.3 ([5]): A suite of actuators is said to be ω-strategic if the excited system is weakly regionally controllable.

Characterizing an actuator by (Ω_i, g_i), see [4], with input area Ω_i and input characteristic g_i, necessary and sufficient conditions for a suit of actuators to be ω-strategic are gathered in the following Theorem.

Theorem 3.4 ([5]): Consider r_n as the multiplicity of the n-th eigenmode. Further, assume that $\sup r_n = r < \infty$, then the suite of actuators $(\Omega_i, g_i)_{1\leq i\leq N_\mathrm{a}}$ is ω-strategic if and only if

1) $N_\mathrm{a} \geq r$
2) $\operatorname{rank}\boldsymbol{G}_n = r_n$

where

$$\boldsymbol{G}_n = \begin{pmatrix} \langle \psi_{n,1}, g_1 \rangle_{L^2(\Omega_1)} & \cdots & \langle \psi_{n,r_n}, g_1 \rangle_{L^2(\Omega_1)} \\ \vdots & & \vdots \\ \langle \psi_{n,1}, g_{N_\mathrm{a}} \rangle_{L^2(\Omega_{N_\mathrm{a}})} & \cdots & \langle \psi_{n,r_n}, g_{N_\mathrm{a}} \rangle_{L^2(\Omega_{N_\mathrm{a}})} \end{pmatrix} \tag{14}$$

A proof to Theorem 3.4 can be found in [5]. Moreover, results from [4] show, that for a given input area of a set of actuators there exist always input characteristics such that an ω-strategic arrangement is achieved and vice versa.

B. Control Lyapunov Function

Based on the introduced assumptions and requirements, a feedback law for controlling a subregion of the plate surface is derived by using a Lyapunov function. Such a stabilizing feedback is stated in the following Theorem.

Theorem 3.5: Consider the system described in (1) with modal solution (8), a subregion $\omega \subseteq \Omega$ with the Assumption 3.1 and ω-strategic actuator locations. Then

$$L(\boldsymbol{x}_\mathrm{e}) = \frac{1}{2}\boldsymbol{x}_\mathrm{e}^\mathsf{T}\left(\boldsymbol{\Psi}^\mathsf{T}\bar{\boldsymbol{S}}\boldsymbol{Q}\bar{\boldsymbol{S}}\boldsymbol{\Psi} - \boldsymbol{\Psi}_{xx}^\mathsf{T}\bar{\boldsymbol{S}}\boldsymbol{Q}\bar{\boldsymbol{S}}\boldsymbol{\Psi}_{yy}\right)\boldsymbol{x}_\mathrm{e}, \tag{15}$$

is a Lyapunov functional and

$$\boldsymbol{u}(\boldsymbol{x}_\mathrm{e}) = k\boldsymbol{B}_\mathrm{e}^{+}\left(\boldsymbol{\Psi}^\mathsf{T}\bar{\boldsymbol{S}}\boldsymbol{Q}\bar{\boldsymbol{S}}\boldsymbol{\Psi} - \boldsymbol{\Psi}_{xx}^\mathsf{T}\bar{\boldsymbol{S}}\boldsymbol{Q}\bar{\boldsymbol{S}}\boldsymbol{\Psi}_{yy}\right)\boldsymbol{A}_\mathrm{e}\boldsymbol{x}_\mathrm{e}, \quad k > 0, \tag{16}$$

is a feedback law that renders the equilibrium $w(t,x,y) = 0 \ \forall \ (x,\ y) \in \omega$ stable in the sense of Lyapunov. The variables in (16) are such that:

$$\boldsymbol{Q} = \begin{pmatrix} \rho h\boldsymbol{I} & 0 \\ 0 & D\boldsymbol{I} \end{pmatrix} \tag{17}$$

$$\begin{aligned}\boldsymbol{\Psi} = &\begin{pmatrix} (0\ \ 1)\otimes(\boldsymbol{\psi}_1\ \ \ldots\ \ \boldsymbol{\psi}_N) \\ (1\ \ 0)\otimes(\boldsymbol{\psi}_{1,\Delta} + \boldsymbol{\psi}_{N,\Delta}) \end{pmatrix} \\ &+ \begin{pmatrix} 0 \\ \left(\sqrt{2(1-\nu)}\ \ 0\right)\otimes(\boldsymbol{\psi}_{1,xy}\ \ \ldots\ \ \boldsymbol{\psi}_{N,xy}) \end{pmatrix}\end{aligned} \tag{18}$$

$$\boldsymbol{\Psi}_{xx} = \begin{pmatrix} 0 \\ \left(\sqrt{2(1-\nu)}\ \ 0\right)\otimes(\boldsymbol{\psi}_{1,xx}\ \ \ldots\ \ \boldsymbol{\psi}_{N,xx}) \end{pmatrix} \tag{19}$$

$$\boldsymbol{\Psi}_{yy} = \begin{pmatrix} 0 \\ \left(\sqrt{2(1-\nu)}\ \ 0\right)\otimes(\boldsymbol{\psi}_{1,yy}\ \ \ldots\ \ \boldsymbol{\psi}_{N,yy}) \end{pmatrix}, \tag{20}$$

with Kronecker product $\otimes$. The vectors $\boldsymbol{\psi}_i$, $\boldsymbol{\psi}_{i,\Delta}$, $\boldsymbol{\psi}_{i,xy}$, $\boldsymbol{\psi}_{i,xx}$ and $\boldsymbol{\psi}_{i,yy}$ of the controlled modes $i \in \{1,\ldots,N\}$ gather the numerical value for each grid point scaled by the square root of each surface segment:

$$\begin{aligned}\boldsymbol{\psi}_i &= \bar{\boldsymbol{A}}\left(\psi_i(x_1,y_1),\ldots,\psi_i(x_{N_\mathrm{g}},y_{N_\mathrm{g}})\right)^\mathsf{T}, \\ \boldsymbol{\psi}_{i,\Delta} &= \bar{\boldsymbol{A}}\left(\psi_{i,\Delta}(x_1,y_1),\ldots,\psi_{i,\Delta}(x_{N_\mathrm{g}},y_{N_\mathrm{g}})\right)^\mathsf{T}, \\ \boldsymbol{\psi}_{i,xx} &= \bar{\boldsymbol{A}}\left(\psi_{i,xx}(x_1,y_1),\ldots,\psi_{i,xx}(x_{N_\mathrm{g}},y_{N_\mathrm{g}})\right)^\mathsf{T}, \\ \boldsymbol{\psi}_{i,yy} &= \bar{\boldsymbol{A}}\left(\psi_{i,yy}(x_1,y_1),\ldots,\psi_{i,yy}(x_{N_\mathrm{g}},y_{N_\mathrm{g}})\right)^\mathsf{T}, \\ \boldsymbol{\psi}_{i,xy} &= \bar{\boldsymbol{A}}\left(\psi_{i,xy}(x_1,y_1),\ldots,\psi_{i,xy}(x_{N_\mathrm{g}},y_{N_\mathrm{g}})\right)^\mathsf{T}, \\ \bar{\boldsymbol{A}} &= \operatorname{diag}\left(\sqrt{A_1},\ldots,\sqrt{A_{N_\mathrm{g}}}\right),\end{aligned}$$

Moreover $\bar{\boldsymbol{S}} = \operatorname{blkdiag}(\boldsymbol{S},\boldsymbol{S})$ is a block diagonal matrix with selection matrix $\boldsymbol{S}$ having a one on its i-th diagonal entry if the grid point (x_i,y_i) is in the subregion ω and zeros elsewhere.

Proof: The kinetic energy T and the potential energy V of

a plate are given by

$$T = \frac{1}{2} m \dot{w}(t,x,y)^2,$$

$$V = \frac{D}{2}\left((\Delta w)^2 + 2(1-\nu) \underbrace{\left(\frac{\partial^2 w}{\partial x \partial y}^2 - \frac{\partial^2 w}{\partial x^2}\frac{\partial^2 w}{\partial y^2} \right)}_{\text{Gauss Curvature}} \right).$$

Summarizing the energy over a plate region ω results in the functional

$$L(\boldsymbol{x}_\mathrm{e}) = \frac{1}{2}\iint_\omega T + V \,\mathrm{d}\omega, \tag{21}$$

which rewrites to

$$L(\boldsymbol{x}_\mathrm{e}) = \frac{1}{2}\iint_\omega \mathscr{E}(x,y,t)\mathrm{d}\omega \tag{22}$$

with

$$\begin{aligned}\mathscr{E}(x,y,t) = m\left(\boldsymbol{\psi}\boldsymbol{S}_{\dot{q}}\boldsymbol{x}_\mathrm{e}\right)^\mathsf{T}\left(\boldsymbol{\psi}\boldsymbol{S}_{\dot{q}}\boldsymbol{x}_\mathrm{e}\right) + D\Big(&\left(\boldsymbol{\psi}_\Delta \boldsymbol{S}_q \boldsymbol{x}_\mathrm{e}\right)^\mathsf{T}\left(\boldsymbol{\psi}_\Delta \boldsymbol{S}_q \boldsymbol{x}_\mathrm{e}\right) \\ &+ 2(1-\nu)\Big(\left(\boldsymbol{\psi}_{xy}\boldsymbol{S}_q\boldsymbol{x}_\mathrm{e}\right)^\mathsf{T}\left(\boldsymbol{\psi}_{xy}\boldsymbol{S}_q\boldsymbol{x}_e\right) \\ &- \left(\boldsymbol{\psi}_{xx}\boldsymbol{S}_q\boldsymbol{x}_\mathrm{e}\right)^\mathsf{T}\left(\boldsymbol{\psi}_{yy}\boldsymbol{S}_q\boldsymbol{x}_\mathrm{e}\right)\Big)\Big)\end{aligned} \tag{23}$$

by substituting $w(x,y,t)$ with (7) and selection matrices $\boldsymbol{S}_q$ and $\boldsymbol{S}_{\dot{q}}$ for the q_i and $\dot{q}_i$ entries of $\boldsymbol{x}_\mathrm{e}$, respectively. Since ω is compact, the plate modes with their partial derivatives are continuous and (23) is bounded for $\boldsymbol{x}_e < \infty$, function (23) is Lebesgue integrable and, thus, Riemann integrable. Evaluating expression (22) over a sufficiently fine grid with N_g points via a Riemann sum leads to

$$L(\boldsymbol{x}_\mathrm{e}) = \frac{1}{2}\boldsymbol{x}_\mathrm{e}^\mathsf{T}\left(\boldsymbol{\Psi}^\mathsf{T}\bar{\boldsymbol{S}}\boldsymbol{Q}\bar{\boldsymbol{S}}\boldsymbol{\Psi} - \boldsymbol{\Psi}_{xx}^\mathsf{T}\bar{\boldsymbol{S}}\boldsymbol{Q}\bar{\boldsymbol{S}}\boldsymbol{\Psi}_{yy}\right)\boldsymbol{x}_\mathrm{e} + \xi, \tag{24}$$

with $\lim_{N\mathrm{g}\to\infty}\xi = 0$ as the residual approximation error. Moreover, (24) is positive for all

$$\boldsymbol{x}_\mathrm{e} \neq \boldsymbol{0} \tag{25}$$

and

$$\boldsymbol{x}_\mathrm{e} \notin \ker\left(\boldsymbol{\Psi}^\mathsf{T}\bar{\boldsymbol{S}}\boldsymbol{Q}\bar{\boldsymbol{S}}\boldsymbol{\Psi} - \boldsymbol{\Psi}_{xx}^\mathsf{T}\bar{\boldsymbol{S}}\boldsymbol{Q}\bar{\boldsymbol{S}}\boldsymbol{\Psi}_{yy}\right), \tag{26}$$

with $\ker(\square)$ as the kernel of $\square$, i.e., the mechanical energy based on (7) not being zero.

Calculating the total time derivative of (24) leads to

$$\begin{aligned}\frac{\mathrm{d}L(\boldsymbol{x}_\mathrm{e}(t))}{\mathrm{d}t} = \boldsymbol{x}_\mathrm{e}^\mathsf{T}\Big(&\boldsymbol{\Psi}^\mathsf{T}\bar{\boldsymbol{S}}\boldsymbol{Q}\bar{\boldsymbol{S}}\boldsymbol{\Psi} - \frac{1}{2}\boldsymbol{\Psi}_{xx}^\mathsf{T}\bar{\boldsymbol{S}}\boldsymbol{Q}\bar{\boldsymbol{S}}\boldsymbol{\Psi}_{yy} \\ &- \frac{1}{2}\boldsymbol{\Psi}_{yy}^\mathsf{T}\bar{\boldsymbol{S}}\boldsymbol{Q}\bar{\boldsymbol{S}}\boldsymbol{\Psi}_{xx}\Big)\dot{\boldsymbol{x}}_\mathrm{e},\end{aligned} \tag{27}$$

which rewrites to

$$\frac{\mathrm{d}L(\boldsymbol{x}_\mathrm{e}(t))}{\mathrm{d}t} = \boldsymbol{x}_\mathrm{e}^\mathsf{T}\left(\boldsymbol{\Psi}^\mathsf{T}\bar{\boldsymbol{S}}\boldsymbol{Q}\bar{\boldsymbol{S}}\boldsymbol{\Psi} - \boldsymbol{\Psi}_{xx}^\mathsf{T}\bar{\boldsymbol{S}}\boldsymbol{Q}\bar{\boldsymbol{S}}\boldsymbol{\Psi}_{yy}\right)\left(\boldsymbol{A}_\mathrm{e}\boldsymbol{x}_\mathrm{e} + \boldsymbol{B}_\mathrm{e}\boldsymbol{u}\right), \tag{28}$$

using $\boldsymbol{\Psi}_{xx}^\mathsf{T}\bar{\boldsymbol{S}}\boldsymbol{Q}\bar{\boldsymbol{S}}\boldsymbol{\Psi}_{yy} = \boldsymbol{\Psi}_{yy}^\mathsf{T}\bar{\boldsymbol{S}}\boldsymbol{Q}\bar{\boldsymbol{S}}\boldsymbol{\Psi}_{xx}$ and replacing $\dot{\boldsymbol{x}}_\mathrm{e}$ by (11). Choosing $\boldsymbol{u} = k\boldsymbol{B}_\mathrm{e}^+\left(\boldsymbol{\Psi}^\mathsf{T}\bar{\boldsymbol{S}}\boldsymbol{Q}\bar{\boldsymbol{S}}\boldsymbol{\Psi} - \boldsymbol{\Psi}_{xx}^\mathsf{T}\bar{\boldsymbol{S}}\boldsymbol{Q}\bar{\boldsymbol{S}}\boldsymbol{\Psi}_{yy}\right)\boldsymbol{A}_\mathrm{e}\boldsymbol{x}_\mathrm{e}$ leaves

$$\begin{aligned}\frac{\mathrm{d}L(\boldsymbol{x}_\mathrm{e}(t))}{\mathrm{d}t} = \boldsymbol{x}_\mathrm{e}^\mathsf{T}\Bigg(&\underbrace{\left(\boldsymbol{\Psi}^\mathsf{T}\bar{\boldsymbol{S}}\boldsymbol{Q}\bar{\boldsymbol{S}}\boldsymbol{\Psi} - \boldsymbol{\Psi}_{xx}^\mathsf{T}\bar{\boldsymbol{S}}\boldsymbol{Q}\bar{\boldsymbol{S}}\boldsymbol{\Psi}_{yy}\right)}_{\succ 0}\underbrace{\boldsymbol{A}_\mathrm{e}}_{\prec 0} \\ &+ k\boldsymbol{B}_\mathrm{e}\boldsymbol{B}_\mathrm{e}^+\left(\boldsymbol{\Psi}^\mathsf{T}\bar{\boldsymbol{S}}\boldsymbol{Q}\bar{\boldsymbol{S}}\boldsymbol{\Psi} - \boldsymbol{\Psi}_{xx}^\mathsf{T}\bar{\boldsymbol{S}}\boldsymbol{Q}\bar{\boldsymbol{S}}\boldsymbol{\Psi}_{yy}\right)\boldsymbol{A}_\mathrm{e}\Bigg)\boldsymbol{x}_\mathrm{e}.\end{aligned} \tag{29}$$

The operator $\square^+$ denotes the Moore-Penrose pseudo inverse of $\square$. Hence, the largest positive invariant subset of $\boldsymbol{x}_\mathrm{e}$ such that $\frac{\mathrm{d}L(\boldsymbol{x}_\mathrm{e}(t))}{\mathrm{d}t} = 0$ comprises

$$\boldsymbol{x}_\mathrm{e} = \boldsymbol{0},$$

and

$$\boldsymbol{x}_\mathrm{e} \in \ker\left(\left(\boldsymbol{\Psi}^\mathsf{T}\bar{\boldsymbol{S}}\boldsymbol{Q}\bar{\boldsymbol{S}}\boldsymbol{\Psi} - \boldsymbol{\Psi}_{xx}^\mathsf{T}\bar{\boldsymbol{S}}\boldsymbol{Q}\bar{\boldsymbol{S}}\boldsymbol{\Psi}_{yy}\right)\boldsymbol{A}_\mathrm{e}\right). \tag{30}$$

Thus, the equilibrium $w(t,x,y) = 0 \;\forall\; (x,\; y) \in \omega$ is Lyapunov stable. ■

Remark 3.6: The expression of the potential energy with partial derivatives with respect to Cartesian coordinates does not restrict the applicability of the presented method to a Cartesian system parameterization, since a different set of coordinates, e.g., polar coordinates, can be easily expressed through Cartesian ones by

$$r(x,y) = \sqrt{x^2+y^2}, \tag{31}$$

$$\varphi(x,y) = \arctan\left(\frac{y}{x}\right). \tag{32}$$

Same holds for different parameterizations like elliptical coordinates.

C. Time varying subregion

During operation, the exposed surface of the considered plate might vary due to changes in the pose of the plate. Hence, the controlled subregion and the feedback law need to be adapted over time. Choosing the previous selection matrix for the plate segments that is used for defining the control law (16) would lead to discontinuities when the center of a segment moves into or out of a time varying subregion $\omega(t)$. Hence, the sigmoid-like selection function

$$\tilde{\boldsymbol{S}}(t) = \mathrm{diag}\left(\alpha_1(t),\ldots,\alpha_{N_\mathrm{g}}(t)\right), \tag{33}$$

with

$$\alpha_i(t) = \begin{cases} 1 & a_i(t) \geq 1, \\ \frac{1}{2} + \frac{1}{2}\cos\left(-\frac{1-a_i(t)}{\gamma}\pi\right), & a_i(t) \in (1-\gamma, 1), \\ 0 & \text{else}, \end{cases} \tag{34}$$

and tolerance factor $\gamma > 0$ is introduced. The scalar $a_i(t)$ denotes the scaling factor from the center of $\omega(t)$ to each center of the plate segments, such that the vector points onto the boundary $\partial\omega(t)$. Using the results of the previous subsection, the following Corollary is deduced from Theorem 3.5.

Corollary 6.1: Consider Assumption 3.1, ω-strategic actuator locations and the selection matrix $\hat{\boldsymbol{S}}(t) = \text{blkdiag}\left(\tilde{\boldsymbol{S}}(t), \tilde{\boldsymbol{S}}(t)\right)$. Then the feedback law

$$\boldsymbol{u}(t) = k\boldsymbol{B}_\text{e}^+ \boldsymbol{\zeta}(t)\boldsymbol{A}_\text{e}\boldsymbol{x}_\text{e}(t) - \boldsymbol{B}_\text{e}^+ \boldsymbol{\zeta}^{-1}(t)\boldsymbol{\Xi}(t)\boldsymbol{x}_\text{e}(t), \tag{35}$$

with $k > 0$ and

$$\begin{aligned}\boldsymbol{\zeta}(t) &= \boldsymbol{\Psi}^\intercal \hat{\boldsymbol{S}}(t)\boldsymbol{Q}\hat{\boldsymbol{S}}(t)\boldsymbol{\Psi} - \boldsymbol{\Psi}_{xx\intercal}\hat{\boldsymbol{S}}(t)\boldsymbol{Q}\hat{\boldsymbol{S}}(t)\boldsymbol{\Psi}_{yy},\\ \boldsymbol{\Xi}(t) &= \boldsymbol{\Psi}^\intercal \hat{\boldsymbol{S}}(t)\boldsymbol{Q}\dot{\hat{\boldsymbol{S}}}(t)\boldsymbol{\Psi} - \boldsymbol{\Psi}_{xx\intercal}\hat{\boldsymbol{S}}(t)\boldsymbol{Q}\dot{\hat{\boldsymbol{S}}}(t)\boldsymbol{\Psi}_{yy},\end{aligned} \tag{36}$$

renders the equilibrium $w(t,x,y) = 0 \;\forall\; (x,\; y) \in \boldsymbol{\omega}(t) \subseteq \Omega$ Lyapunov stable.

Proof: The proof follows the same steps as the one of Theorem 3.5 up to equation (26). Considering a time dependent selection matrix changes the total time derivative of the Lyapunov functional to

$$\frac{\mathrm{d}L(\boldsymbol{x}_\text{e}(t))}{\mathrm{d}t} = \boldsymbol{x}_\text{e}^\intercal(t)\boldsymbol{\zeta}(t)\left(\boldsymbol{A}_\text{e}\boldsymbol{x}_\text{e}(t) + \boldsymbol{B}_\text{e}\boldsymbol{u}(t)\right) + \boldsymbol{x}_\text{e}^\intercal(t)\boldsymbol{\Xi}(t)\boldsymbol{x}_\text{e}(t). \tag{37}$$

By replacing $\boldsymbol{u}(t)$ with (35) and considering analogous steps as in the proof of Theorem 3.5 the proof is completed. ■

IV. Simulation

Based on the results from Section III, a simulation study of a thin circular plate with free edge, see Figure 3, is conducted. The governing PDE of the considered thin circular plate is given by

$$D\Delta\Delta w + Q_\text{d} + \rho h\frac{\partial^2 w}{\partial t^2} = Q_a,\;\; t > 0,\;\; (r,\varphi) \in \Omega, \tag{38a}$$

$$\mathscr{M} w = 0,\;\; t > 0,\;\; (r,\varphi) \in \partial\Omega, \tag{38b}$$

$$\mathscr{V} w = 0,\;\; t > 0,\;\; (r,\varphi) \in \partial\Omega, \tag{38c}$$

$$w = \frac{\partial w}{\partial t} = 0 \;\text{ for }\; t = 0,\;\; (r,\varphi) \in \Omega, \tag{38d}$$

with a damping term

$$Q_\text{d}(r,\varphi,t) = (\lambda_\text{d} + \kappa_\text{d}\Delta\Delta)\frac{\partial w(r,\varphi,t)}{\partial t} \tag{39}$$

covering viscous and structural damping via the coefficients λ_d and κ_d, respectively, and the external forces

$$\begin{aligned}Q_\text{a}(r,\varphi,t) = &\sum_{i=1}^{N_\text{a}} \frac{u_i(t)}{r_{\text{a},i}}\delta(r - r_{\text{a},i})\delta(\varphi - \varphi_{\text{a},i}),\\ &+ \sum_{i=1}^{N_\text{dist}} \frac{u_{\text{dist},i}(t)}{r_{\text{dist},i}}\delta(r - r_{\text{dist},i})\delta(\varphi - \varphi_{\text{dist},i})\end{aligned} \tag{40}$$

with delta distribution $\delta(\cdot)$, actuator forces $u_i(t)$ and disturbing forces $u_{\text{dist},i}(t)$. The location of the actuators are chosen such that the conditions on an ω-strategic placement are fulfilled. A solution to system (38) can be found in various literature, e.g., [13]. Numerical values of the material parameters, the shape of the plate and number of actuators are listed in Table I.

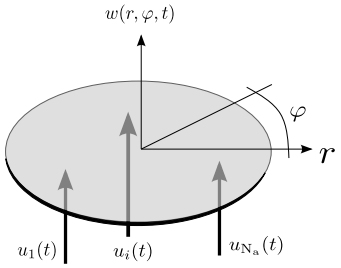

Fig. 3. Thin circular plate with point wise forces $u_i(t)$.

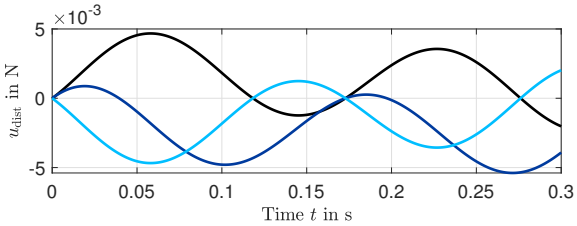

Fig. 4. Disturbing forces acting point wise and perpendicular to the plate's surface.

A. Comparison to linear quadratic regulator

In a first step, the proposed feedback law (16) is compared to a linear quadratic regulator (LQR), as an established method for the control with a state feedback. Comparison takes place between the regulator K_Ω and K_ω based on (16), whereby K_Ω considers the whole plate surface Ω and K_ω only the subregion ω. The weighting matrices for the LQR synthesis are set to

$$\boldsymbol{Q}_\text{LQR} = \boldsymbol{\Psi}^\intercal\boldsymbol{Q}\boldsymbol{\Psi} - \boldsymbol{\Psi}_{xx}^\intercal\boldsymbol{Q}\boldsymbol{\Psi}_{yy},\;\; \boldsymbol{R}_\text{LQR} = \frac{1}{k}\boldsymbol{I}. \tag{41}$$

The performance of all three control laws is evaluated by the root-mean-square (RMS) error over $\boldsymbol{\omega} = \left[0, \frac{R}{2}\right] \times [0, 2\pi)$ defined by

$$w_{\text{RMS}_\omega}(t) = \sqrt{\frac{1}{A_\omega}\iint_\omega w^2(r,\varphi,t)\mathrm{d}\omega}, \tag{42}$$

with surface A_ω covered by ω and normalized with the largest value occurring during the simulation. Additionally, the plate is excited by three disturbing forces, whose course of time is portrayed in Figure 4. For the considered simulation set up, the first $N = 10$ modes are controlled whereas the plant model covers the first fifteen plate modes.

TABLE I
Parameters of the thin circular plate.

Parameter	Value
E	$210\,\text{GN}\,\text{m}^{-2}$
ν	0.3
ρ	$7850\,\text{kg}\,\text{m}^{-3}$
h	0.01 m
R	0.5 m
λ_d	$10\,\text{N}\,\text{s}\,\text{m}^{-3}$
κ_d	$1\,\text{N}\,\text{s}\,\text{m}$
N_a	20
N_dist	3

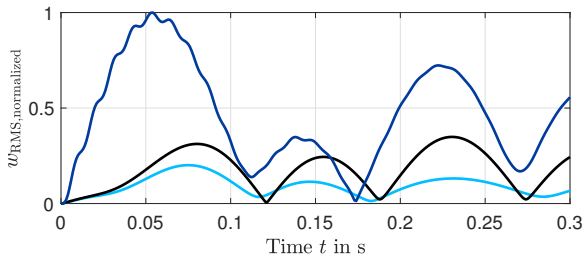

Fig. 5. Comparison of a LQR (—) and controller for the regions ω (—) and Ω (—) based on (16 whose performance is evaluated by the RMS-error over the subregion ω.

Figure 5 shows the results. Evidently, the LQR leads to the largest RMS errors and is, thus, outperformed by the derived feedback law (16). Moreover, considering only the relevant region ω decreases the RMS error even further, which underlines the effectiveness of the presented method.

B. Time varying control

Next, the proposed control law (35) is evaluated. The time varying subregion is defined through

$$\omega(t) = [0, r_\omega(t)] \times [0, 2\pi), \tag{43}$$

with

$$r_\omega(t) = r_0 + \tilde{r}\sin(\frac{2\pi}{T}t), \tag{44}$$

The time dependent radius$r_\omega(t)$ is parameterized by the offset radius $r_0 = \frac{R}{2}$, radial amplitude $\tilde{r} = 0.3R$ and period $T = 0.3$ s. Again, the plate is excited by three disturbing forces displayed in Figure 4.

Figure 6 shows the largest real part of the closed loop poles. During the change of $\omega(t)$, the largest real part remains negative. Thus, applying the control signal (16) to the plant leads to a stable closed loop for the varying subregion.

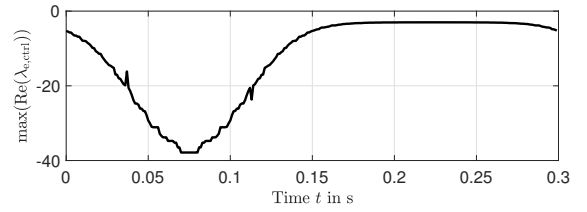

Fig. 6. Maximum real part of the closed loop poles for the controlled plate modes of system (38) with feedback law (35) for varying subregion (43).

V. CONCLUSIONS AND FUTURE WORKS

A. Conclusions

Based on the modal solution to the PDE of a general thin vibrating plate, a stabilizing state feedback for the control of a subregion is derived. Stability of the proposed method is shown via the direct method of Lyapunov with a Lyapunov functional that is deduced from the mechanical plate energy over the controlled subregion by evaluating discrete surface segments. The method is then extended to a time varying subregion by introducing a time dependent matrix for selecting required surface segments based on a sigmoid-like selection function. Effectiveness of the proposed method is then shown for a fixed subregion on a thin circular plate through comparison with an LQR. Simulation results show a significant improvement over the LQR. Finally, stability of the closed loop for the time varying control law is validated in a numeric evaluation.

B. Future Works

The Lyapunov functional is deduced form the mechanical plate energy by using an approximation of the surface deflection by a truncated modal synthesis and a Riemann sum for the integrals. In order to improve the control law for a time varying subregion, an exact evaluation of the integral should be considered. Moreover, higher order modes are simply neglected in (7), this might result in a spillover effect. Hence, future work should address a control synthesis for a time varying subregion directly from the PDE, to cover all plate modes at once.

REFERENCES

[1] Abderrahman Ait Aadi et al. Regional optimal control of a bilinear plate equation. In *2019 6th International Conference on Control, Decision and Information Technologies (CoDIT)*, pages 349–354. IEEE, 2019.

[2] Abderrahman Ait Aadi and El Hassan Zerrik. Constrained regional control problem of a bilinear plate equation. *International Journal of Control*, 95(4):996–1002, 2022.

[3] Patricia Daukantas. Ground-based telescopes for the 21 st century. *Optics and photonics news*, 18(9):28–34, 2007.

[4] A El Jai. Distributed systems analysis via sensors and actuators. *Sensors and Actuators A: Physical*, 29(1):1–11, 1991.

[5] Abdelhaq El Jai, Marie-Claude Simon, E Zerrik, and AJ Pritchard. Regional controllability of distributed parameter systems. *International Journal of Control*, 62(6):1351–1365, 1995.

[6] Timothy G Hawarden. Extremely large ground-based telescopes (elts): Performance comparisons with 8-m class space telescopes. *The Institute of Space and Astronautical Science Report SP*, (14):249–256, 2000.

[7] Xuezhang Hou. A variable structural control for a flexible plate.

[8] Miroslav Krstic, Antranik A Siranosian, and Andrey Smyshlyaev. Backstepping boundary controllers and observers for the slender timoshenko beam: Part i-design. In *2006 American Control Conference*, pages 2412–2417. IEEE, 2006.

[9] Miroslav Krstic, Antranik A Siranosian, Andrey Smyshlyaev, and Matt Bement. Backstepping boundary controllers and observers for the slender timoshenko beam: Part ii—stability and simulations. In *Proceedings of the 45th IEEE Conference on Decision and Control*, pages 3938–3943. IEEE, 2006.

[10] Stephen Shectman and Matt Johns. Gmt overview. In *Ground-based and Airborne Telescopes III*, volume 7733, pages 704–714. SPIE, 2010.

[11] Ali Tavasoli. Robust boundary stabilization of a vibrating rectangular plate using disturbance adaptation. *International Journal of Adaptive Control and Signal Processing*, 30(11):1603–1626, 2016.

[12] Ali Tavasoli and Vali Enjilela. Active disturbance rejection and lyapunov redesign approaches for robust boundary control of plate vibration. *International Journal of Systems Science*, 48(8):1656–1670, 2017.

[13] Andrei Zagrai and Dimitri Donskoy. A "soft table" for the natural frequencies and modal parameters of uniform circular plates with elastic edge support. *Journal of Sound and Vibration*, 287(1-2):343–351, 2005.